28p

NASA TN D-1728

TECHNICAL NOTE

D-1728

RATE OF LIQUID JET BREAKUP BY A TRANSVERSE SHOCK WAVE

By Gerald Morrell

Lewis Research Center
Cleveland, Ohio

NATIONAL AERONAUTICS AND SPACE ADMINISTRATION

WASHINGTON

May 1963

NATIONAL AERONAUTICS AND SPACE ADMINISTRATION

TECHNICAL NOTE D-1728

RATE OF LIQUID JET BREAKUP BY A TRANSVERSE SHOCK WAVE

By Gerald Morrell

SUMMARY

The breakup of a single water jet by a transverse shock was studied experimentally in a 2.7- by 2.7-inch shock tube equipped with a variable-length high-pressure section. High-speed backlighted photographs were analyzed to obtain breakup time and liquid deformation.

Breakup time decreased regularly with an increase in gas velocity and increased with jet radius. The extent of deformation was a linear function of the ratio of Weber number to the square root of Reynolds number based on initial jet radius.

A theoretical model was developed based on stripping from a liquid-phase boundary layer, and an explicit function for breakup time resulted. The calculated breakup times were found to be in fair agreement with the measured values.

INTRODUCTION

An important problem in combustion theory and practice is to establish the response of a burning system to a pressure or velocity disturbance. In rocket engines, for example, the response can take the form of an oscillatory mode of burning with undesirable side effects such as destructive mechanical vibrations and intolerable heat flux rates. For particular geometries, the conservation equations can be solved to obtain the predicted response to a disturbance provided a controlling heat release process is assumed and a rate law is available for this process (refs. 1 and 2).

The objective of the research reported herein was to study such a process, jet breakup by shock waves, with a view to obtaining a better understanding of the fluid mechanics involved and a rate law that might be used to describe the growth of a disturbance in a combustion system composed of burning sprays or jets. Interest in such a process stems from the elementary consideration that, in a combustion system in which the rate of burning is determined by the vaporization rate of the reactants, any disturbance that increases the liquid surface area will be amplified if the increase is rapid enough. Indirect evidence from several combustion experiments (refs. 3, 4, and 5) indicates that jet and drop shattering can, in fact, produce local increases in heat release rate and amplify shock waves. Further evidence is found in reference 6, which shows that an index of rocket engine stability can be obtained by employing a jet- or drop-shattering process with the conservation equations. An analysis of the existing data on the

critical conditions for jet and drop shattering (ref. 7) indicates that there is a predictable velocity at which breakup commences and that this velocity is a function of the liquid dimensions and properties and the duration of the flow. In short, it appears that jet or drop shattering may be a rate process that can account for the growth and propagation of a wave in a liquid-fuel combustion system that is vaporization limited. The finite amplitude required to initiate the process, however, appears to rule out its application to the intrinsic form of instability discussed in reference 8.

In a previous study (ref. 9) the breakup of liquid jets by short-duration shock waves was examined, but the limited range of experimental conditions possible did not permit a definitive test of the proposed theoretical model. In this study experiments were conducted in a shock tube with a variable-length high-pressure section to obtain breakup time as a function of jet diameter, gas particle velocity behind the shock, and flow duration. Breakup times were deduced from backlighted high-speed motion pictures and streak photographs. These times were compared with those predicted from the previously derived model and a new model based on streaming from a liquid boundary layer.

APPARATUS AND EXPERIMENTAL METHOD

The shock tube consisted of the usual components: high-pressure section, diaphragm holder, test section, and downstream expansion section. Instrumentation was provided for measuring wave velocity and pressure behind the wave. The entire assembly was mounted on a U-beam supported on A-frames attached to concrete pedestals. The sections downstream of the diaphragm holder were clamped to the U-beam, but the high-pressure section could be rolled back to permit installation of diaphragms. A schematic of the shock tube is shown in figure 1(a).

High-Pressure Section

By bolting together various lengths of 3-inch-diameter schedule 40S pipe, the high-pressure section could be varied in length from 6 inches to 8 feet. By using internal blocks, the length could be reduced to as little as 1 inch. An axially supported rod and striker assembly was used to pierce the diaphragm. The assembly was attached to a gas-operated piston actuator located at the end of the high-pressure section.

Diaphragm Holder

The diaphragms were clamped to the downstream flange of the high-pressure section by a 9-inch-diameter holder with a length of 1.75 inches and a bore of 3.086 inches (the actual diameter of the pipe). A 16-thread-per-inch spiral groove was applied to the surface of the bore to prevent the diaphragm "petals" from springing back after rupture. Actual sealing of the diaphragm was accomplished by O-rings on the flange and holder.

Test Section

A 6-inch-long transition piece was installed between the diaphragm holder and the square test section, which had an internal dimension of 2.721 inches and a length of 6 feet. The liquid injector centerline was 51.5 inches from the diaphragm location and provided a run length of 16.7 diameters. A 1.25-inch-diameter opening in the floor of the test section permitted the jet to flow directly through. The portion of the test section in the vicinity of the injector was provided with flat optical glass windows, which gave a viewing area of 2.72 by 14 inches that extended from 2 inches upstream of the injector centerline to 12 inches downstream. The dimensions of the test section were chosen to give a cross-sectional area approximately equal to that of the 3-inch pipe so as to minimize the possible disturbances due to the transition from a circular to square cross section.

Following the test section was a second transition section, 6 inches long, and an $8\frac{1}{2}$-foot length of 3-inch-diameter schedule 40S pipe, which was the expansion section. The latter was sufficiently long that for most runs the reflected wave from the end of the high-pressure section arrived at the injector station before the wave from the end of the expansion section.

Instrumentation

Wave speed was measured by two barium titanate transducers located 2 feet apart and mounted at a 45° angle with respect to the direction of motion. One gage was mounted 8 inches upstream of the injector centerline, and the other was 16 inches downstream. The pressure behind the wave was monitored by a high-frequency-response strain-tube pressure transducer with a natural frequency of approximately 25 kilocycles and a range of 200 pounds per square inch. This gage was mounted 11 inches downstream of the injector. A 1-kilocycle electronic tuning fork provided the time base. The signals from these instruments were displayed by a two-beam oscilloscope equipped with 100-kilocycle chopping amplifiers to produce four displays on a time-sharing basis. The oscilloscope was operated in the nonsweeping mode, with the sweep function supplied by the camera as described in the following section.

Photography

The test section in the vicinity of the jet was backlighted by a 100-watt concentrated arc lamp and a 6-inch-diameter, 12-inch-focal-length condensing lens. Two types of photographic data were obtained. A twin-lens 35-mm high-speed camera was used to obtain motion pictures of the breakup process at a rate of approximately 2000 frames per second. The second lens, operating without a shutter, recorded the amplitudes of the pressure and time signals displayed on the oscilloscope so that the film motion (1540 in./sec) provided the sweep function. The motion pictures were taken with a 100-mm, f/3.5 lens, with a demagnification of 9.25, and with a 50-mm, f/2 lens, with a demagnification of 10.

Streak photographs were taken with a 35-mm shutterless high-speed camera at 990 inches per second. In this case the test section window facing the camera

was masked except for an axial slit 0.25 mm wide and 14 inches long. The oscilloscope display was photographed simultaneously by means of a mirror arrangement. For these photographs a 50-mm f/2 lens was used with a demagnification of 11. Examples of both types of photographs are shown in figure 2.

The film data were read on a motion analyzer equipped with precision cross hairs that provided a magnification of 5. The estimated error in shock velocity was about 1 percent, and for pressure the error was estimated to be about 3 percent. The error in estimating breakup time was considerably larger. Since atomization occurs throughout the breakup period, the spray that is formed tends to obscure the liquid that has not yet been atomized; thus, some judgment was required to establish the terminal point of the process. Comparisons among the photographic methods, the exposure, and the estimates of different observers for a series of replicate runs indicate an error of about 20 percent in breakup time. A large number of runs was required, therefore, to establish trends.

Range of Experiments

Four jet diameters were included in the study (0.018, 0.052, 0.0785, and 0.157 in., see fig. 1(b)). The length to diameter ratio of each injector was at least 10. Although the injectors were designed with two jets to permit mixing studies, only one of the jets was used for these experiments. An additional injector shown in figure 1(c) was also used. This consisted of a 0.052-inch-diameter sharp-edged orifice mounted on the end of a large plenum. Overall pressure drop for the liquid system was held constant at 40 pounds per square inch gage; jet velocities, as determined by volumetric calibration, ranged from 20 to 46 feet per second, depending on jet diameter. Gas velocities behind the shock wave were not less than three times the liquid velocities in all cases where breakup times were measured.

The initial pressure in the test section was always 1 atmosphere, and four values of initial pressure ratio (across the diaphragm) were used. These values together with the diaphragm materials are shown in the following table:

Initial pressure ratio	Nominal shock Mach number	Diaphragm material	Diaphragm thickness
1.68	1.115	Oiled onion-skin paper	2 Sheets
2.63	1.225	Soft brass	0.0015 In.
7.12	1.506	Soft brass	.004 In.
14.61	1.725	Spring brass	.007 In.

The pressure ratios shown were 80 to 90 percent of the experimental values required to burst the diaphragms.

High-pressure-section lengths of 1 inch, 6 inches, 2 feet, and 8 feet were used to vary the duration of gas flow behind the shock wave. This flow duration,

or action time, was taken for this study as the time required for the pressure behind the shock to decay to one-third of its initial value.

Experimental Procedure

The method followed for each experiment with a particular length of high-pressure section and a given injector size was as follows: After the unscored diaphragm was clamped in place, the upstream section was pressurized with dry nitrogen and isolated by closing the inlet valve. The water flow was started; when the jet appeared to have stabilized, the oscilloscope was switched to the unswept mode, and the camera was started. After a delay of 0.7 second, to permit the camera to reach constant speed, a relay actuated the piercing mechanism, and the ensuing action was photographed.

The gas velocity behind the shock wave u and the density ratio across the shock ρ/ρ_1 were calculated from the one-dimensional shock-wave equations (ref. 10) using a temperature of 70° F for estimating sound speed in the undisturbed gas. (Symbols are defined in the appendix.) The actual ambient temperature recorded in the laboratory was 70°±5° F.

The physical properties used for air and water were literature values at 70° F and 1-atmosphere pressure: initial air density ρ_1, 0.07488 pound per cubic foot; liquid density ρ_l, 62.4 pounds per cubic foot; gas viscosity μ, 1.205×10^{-5} pound per foot per second; liquid viscosity μ_l, 6.72×10^{-4} pound per foot per second; and interfacial tension σ, 73 dynes per centimeter (0.161 lb/sec^2).

RESULTS

The primary experimental data and pertinent calculated parameters are presented in table I. Except for the 1-inch high-pressure section, the observed shock speeds agree within 5 percent with those calculated from the initial pressure ratio by the one-dimensional-flow equations.

Typical frame and streak photographs from which breakup times were obtained are shown in figure 2. Examples of the dependence of breakup time on gas velocity are shown by the plots of figure 3, which are based on streak photographic data.

The data indicate a monotonic decrease in breakup time with increasing gas velocity. No explanation has been found for the few exceptions. It is also apparent that the duration of flow behind the shock wave (action time) t_a has some bearing on the process of breakup. For sufficiently short action times breakup is incomplete, otherwise there appears to be little effect on observed time.

Although measurement of the threshold gas velocity for breakup was not a subject of this study, the few instances where breakup was incomplete provide an estimate. The theoretical values calculated from reference 7 for a stagnation-point deflection of unity appear to be lower limits as seen in figure 3. The experimental thresholds seem to follow a different trend, which indicates a depend-

ence of critical velocity on the initial radius that was not included in the theoretical treatment.

The observed breakup seems to occur by at least two processes as shown in the examples of figure 2. There appears to be a general deformation with breaks occurring at various locations. The bulk of the liquid appears to form a sheet of considerable thickness as observed in the streak photographs. Simultaneously, there occurs a continual streaming of finely atomized material from the surface. Similar behavior of single drops has been observed in other studies (e.g., ref. 11). The rate controlling process cannot be determined from the photographs alone; however, the deformation process appears to be predominant near the threshold velocity for breakup, and the atomization process appears to become increasingly important as the velocity increases.

The data presented in table I are for turbulent jets characterized by surface irregularities. To test the influence of these irregularities on the breakup rate, a series of experiments was conducted with smooth 0.052-inch-diameter jets produced by a sharp-edged orifice (fig. 1(c)). The results are shown in table II.

In figure 4, the breakup times of the smooth jets are compared with the times obtained under the same conditions for turbulent jets. There appears to be little difference between the two sets of data, which indicates that jet turbulence has little effect on the breakup process where the relative velocity is high.

THEORETICAL MODELS

From the experimental observations, two alternate models for the breakup process are suggested: (1) atomization by stripping of a liquid boundary layer, and (2) deformation of the liquid mass. Actually, both processes appear to be taking place simultaneously, but for the purposes of this analysis they are treated independently.

Atomization Model

In reference 12, it was shown that an atomization model based on lenticular drop formation and an exponential velocity profile in the liquid boundary layer could not account for the observed threshold conditions for drop shattering. Although the photographs of drop breakup in high-velocity flows might be interpreted on the basis of lenticular drop formation (e.g., ref. 11), it is just as likely that a thin-walled hollow cylinder of liquid is formed that obscures the actual shape of the liquid mass. Examination of the streak photographs obtained in this study suggests that the liquid mass is deformed either into a single liquid sheet starting at the stagnation point or into two liquid sheets issuing from the lines of tangency with the flow vector. In any event, the atomization may be considered to occur along two surfaces parallel to the gas flow vector, as shown in the following sketch:

Original jet cross section

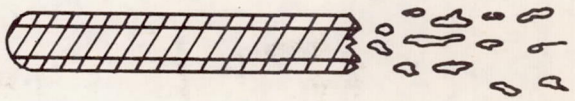

Elongated cross section formed during breakup process (enlarged)

The volumetric removal rate may be written

$$-\frac{dV}{dt} = (2\delta_l u_{l,av})\Big|_{x=L} \tag{1}$$

where V is the volume of liquid per unit length of jet, t is the time, δ_l is the thickness of the liquid boundary layer, $u_{l,av}$ is the arithmetic average velocity in the boundary layer, x is distance along the sheet, and L is the length of the sheet. For constant L and free-stream gas velocity, $(\delta_l u_{l,av})\Big|_{x=L}$ may be considered constant, and equation (1) may be integrated to yield

$$t_b = \frac{\pi R_0^2}{(2\delta_l u_{l,av})\Big|_{x=L}} \tag{2}$$

where R_0 is the initial jet radius and t_b is the breakup time. Evaluation of equation (2) requires a knowledge of the boundary-layer thickness and velocity and the length of sheet formed.

A force balance on a liquid sheet, which equates friction drag according to Blasius with surface tension force, indicates that sheet length should be a function of $We_0/\sqrt{Re_0}$, where We_0, the Weber number, $R_0 u^2 \rho/\sigma$, is based on the initial radius of the jet, as is Re_0, the Reynolds number, $R_0 u\rho/\mu$, and where u is the gas velocity, ρ is gas density, μ is gas viscosity, and σ is interfacial tension. A plot of maximum apparent sheet lengths obtained from streak pictures is plotted in figure 5 as a function of $We_0/\sqrt{Re_0}$. It can be seen that the data are reasonably well represented by the equation:

$$L = 2R_0\left(1 + 2\frac{We_0}{\sqrt{Re_0}}\right) \tag{3}$$

The boundary-layer velocity and thickness can be estimated by assuming a

flat-plate configuration and applying von Karman's boundary-layer momentum theorem for the liquid:

$$\frac{d}{dx}\int_0^{\delta_l} u_l^2\, dy = -\nu_l \left(\frac{\partial u_l}{\partial y}\right)_{y=0} \tag{4}$$

and for the gas phase:

$$\frac{d}{dx}\int_0^{\delta_g} u_g(u - u_g)dy = \nu_g \left(\frac{\partial u_g}{\partial y}\right)_{y=0} \tag{5}$$

where y is measured positively in both directions from the interface, ν is the kinematic viscosity, u is the free-stream velocity (calculated velocity behind the shock wave), u_l and u_g are the respective velocities in the liquid and gas boundary layers, and δ is boundary-layer thickness. We assume also that the boundary-layer flow is laminar:

$$\delta_l = \alpha_l \sqrt{x} \tag{6}$$

and

$$\delta_g = \alpha_g \sqrt{x} \tag{7}$$

where α_l and α_g are to be determined, and that the shear stresses are balanced at the interface:

$$\tau_w = -\mu_l \left(\frac{\partial u_l}{\partial y}\right)_{y=0} = \mu_g \left(\frac{\partial u_g}{\partial y}\right)_{y=0} \tag{8}$$

where τ_w is the interface shear stress.

For the velocity profiles, we adopt a modified form of the general profile suggested in reference 13:

$$\frac{u_g}{u} = 1 - (1 - A)\left[1 - \left(\frac{y}{\delta_g}\right)\right]^2 \tag{9}$$

and

$$\frac{u_l}{u} = A\left[1 - \left(\frac{y}{\delta_l}\right)\right]^2 \tag{10}$$

This selection assures that the velocity will be continuous at the interface,

since for $y = 0$, $u_l = u_g = uA$. The value of A is to be determined by the solution, which is obtained by substituting equations (6) to (10) in equations (4) and (5). The solution is:

$$A = \frac{20\nu_l}{\alpha_l^2 u} = \frac{20\nu_g}{\alpha_g^2 u} - \frac{2}{3} \tag{11}$$

and

$$\frac{\tau_w \sqrt{x}}{u} = \frac{\rho_l \nu_l}{\alpha_l}\left(\frac{40\nu_l}{\alpha_l^2 u}\right) = \frac{\rho_g \nu_g}{\alpha_g}\left(\frac{10}{3} - \frac{40\nu_g}{\alpha_g^2 u}\right) \tag{12}$$

Let $\xi = \nu_g/\alpha_g^2 u$ and $\lambda = \nu_l/\alpha_l^2 u$, and equations (11) and (12) become:

$$20\lambda = 20\xi - \frac{2}{3} \tag{13}$$

and

$$\frac{\rho_l \nu_l^{1/2}}{\rho_g \nu_g^{1/2}} \lambda^{3/2} = \frac{1}{12} \xi^{1/2} - \xi^{3/2} \tag{14}$$

Assume $\xi \gg \lambda$, which is usually the case; then equation (13) yields $\xi \approx 1/30$, and equation (14) yields $\lambda = 0.043(\rho_g/\rho_l)^{2/3}(\nu_g/\nu_l)^{1/3}$, which is almost an order of magnitude smaller than the value obtained in reference 12. The boundary-layer thickness is given by

$$\delta_l = \sqrt{\frac{\nu_l x}{\lambda u}} \tag{15}$$

and the average boundary-layer velocity is given by

$$u_{l,av} = 10\lambda u \tag{16}$$

Substitution of equations (15) and (16) in equation (2) yields

$$t_b = \frac{\pi R_0^2}{20\lambda u \sqrt{\frac{\nu_l L}{\lambda u}}}$$

$$= \frac{\pi R_0^2}{20\sqrt{2\lambda u \nu_l R_0 \left(1 + 2\,\frac{We_0}{\sqrt{Re_0}}\right)}}$$

$$= 0.536\left(\frac{\rho_l}{\rho}\right)^{2/3}\left(\frac{\mu}{\mu_l}\right)^{1/3}\frac{R_0}{u}\sqrt{\frac{Re_0}{1 + 2\,\frac{We_0}{\sqrt{Re_0}}}} \qquad (17)$$

where $Re_0 \equiv R_0 u\rho/\mu$ and $We_0 \equiv R_0 u^2 \rho/\sigma$. Equation (17) does not take into account the action time of the flow behind the shock wave t_a. The simplest behavior that can be assumed is that, if $t_b > t_a$, breakup will not be complete and that the fraction of mass atomized will be t_a/t_b; that is, the rate of breakup is constant. For the case that $We_0/\sqrt{Re_0} \gg 1$, the dependence of t_b on R_0 and u is given by:

$$t_b \propto \left(\frac{R_0}{u}\right)^{1.25}$$

Deformation Model

An alternative way to examine the breakup process is to assume that the observed liquid mass represents the deformed jet and that when the deformation becomes sufficiently large, interfacial tension forces will cause the mass to break into small fragments. In this study, such behavior appeared to be the dominant mode of breakup near the velocity threshold.

In a previous study (ref. 9) the following expression was derived for the deformation of a liquid cylinder subjected to a shock wave:

$$\frac{\frac{\Delta}{R_0}}{\frac{\rho u^2 R_0}{\sigma}} = 0.092\left[\frac{e^{-t_b/t_a} + \frac{\sin \omega_2 t_b}{\omega_2 t_a} - \cos \omega_2 t_b}{1 + \left(\frac{1}{\omega_2 t_a}\right)^2}\right]$$

$$+ 0.026\left[\frac{e^{-t_b/t_a} + \frac{\sin \omega_3 t_b}{\omega_3 t_a} - \cos \omega_3 t_b}{1 + \left(\frac{1}{\omega_3 t_a}\right)^2}\right]$$

$$+ 0.006\left[\frac{e^{-t_b/t_a} + \frac{\sin \omega_4 t_b}{\omega_4 t_a} - \cos \omega_4 t_b}{1 + \left(\frac{1}{\omega_4 t_a}\right)^2}\right] \qquad (18)$$

where Δ is the displacement of the stagnation point due to the deformation process, and

$$\omega_n = \sqrt{\frac{n(n^2 - 1)\sigma}{\rho_l R_0^3}}$$

The experimental data indicated that a constant value of Δ/R_0 corresponding to breakup could only be assumed for the threshold condition. For all other cases, Δ/R_0 appeared to vary with Weber number and to have large values inconsistent with the small perturbation assumption of the mathematical derivation.

For purposes of this analysis, we may assume that the observed elongation of mass represents the deformation Δ, so that, according to equation (3),

$$\frac{\Delta}{R_0} = 2 + 4\frac{We_0}{\sqrt{Re_0}}$$

Substitution of this expression in the left side of equation (18) yields:

$$\frac{2}{We_0} + \frac{4}{\sqrt{Re_0}} = 0.092\left[\frac{e^{-t_b/t_a} + \frac{\sin \omega_2 t_b}{\omega_2 t_a} - \cos \omega_2 t_b}{1 + \left(\frac{1}{\omega_2 t_a}\right)^2}\right]$$

$$+ 0.026\left[\frac{e^{-t_b/t_a} + \frac{\sin \omega_3 t_b}{\omega_3 t_a} - \cos \omega_3 t_b}{1 + \left(\frac{1}{\omega_3 t_a}\right)^2}\right]$$

$$+ 0.006\left[\frac{e^{-t_b/t_a} + \frac{\sin \omega_4 t_b}{\omega_4 t_a} - \cos \omega_4 t_b}{1 + \left(\frac{1}{\omega_4 t_a}\right)^2}\right] + \ldots \qquad (18a)$$

This expression is plotted in figure 6. The maximum point on each curve represents the breakup time corresponding to the threshold gas velocity.

DISCUSSION

In figure 7(a) are plotted the measured breakup times as a function of the values calculated from equation (17). When the lack of precision of the experimental data is considered, the agreement between theory and experiment seems satisfactory. It is also interesting to note that, for calculated values of t_b greater than t_a, the breakup process tends to be incomplete as predicted previously. Equation (17) tends to give high results near the threshold (large values of t_b), but this is the region in which it was noted that a deformation process appears to be dominant.

Values of t_b as given by equation (18a) are plotted in figure 7(b) and compared with the experimental values. The theory, in this case, always predicts low values of t_b, and the breakup tends to be incomplete even for cases where the calculated value of t_b is less than t_a.

For the moment it appears that equation (17) is to be preferred for predicting breakup times of single jets even though the result is likely to be high near the threshold velocity. However, since only one fluid and one level of ambient pressure were studied, it cannot be said that the theory has had a rigorous experimental test.

If it is assumed that equation (17) has general validity, its implications for combustion systems may be examined. For example, as shown in reference 2 we may relate the fraction burned per unit length m to the breakup time by considering that the burning rate becomes essentially equal to the breakup rate:

$$m \propto \frac{1}{t_b V_j}$$

where V_j is jet velocity. Thus, the stability of a system can be assessed when jet shattering is the driving force. In using reference 2, however, it is assumed that the process of jet shattering produces a new quasi-steady heat release rate.

Alternatively, we may ask what is the amplitude of the perturbation in heat release rate behind a shock wave and how is this amplitude related to system stability. As a first approximation the perturbation may be written as t_a/t_b, and, in the absence of an exact system analysis, it can be expected that scaling for stability should be based on maintaining t_a/t_b constant. Suppose, for example, it is desired to scale a rocket to a larger thrust level by maintaining the average flow per unit cross section constant and increasing combustor diameter and to maintain stability with respect to transverse modes of oscillation. As t_a is now larger, t_b must be increased by increasing R_0, since from equation (17) $t_b \propto R_0^{1.25}$. Again, suppose it is desired to scale to larger thrust by maintaining dimensions constant but increasing flow rate and hence pressure in the reactor. In this case, t_a will remain essentially constant, and t_b must be held constant. From equation (17), $t_b \propto R_0^{1.25}/\rho_g^{0.42}$, and jet radius should be increased to compensate for the effect of increased combustion pressure.

SUMMARY OF RESULTS

Breakup of water jets in a transverse shock wave was studied in a 2.7- by 2.7-inch shock tube with a variable-length high-pressure section. Breakup times derived from high-speed photographs decreased monotonically with gas velocity behind the shock and increased monotonically with jet radius.

Fair agreement between theory and experiment was obtained by assuming streaming from a liquid boundary layer to be the rate determining process, and an analytical expression is presented for calculating breakup time.

Lewis Research Center
National Aeronautics and Space Administration
Cleveland, Ohio, February 15, 1963

APPENDIX - SYMBOLS

L	length of sheet
m	fraction burned per unit length
R_0	initial jet radius
Re_0	Reynolds number based on R_0, $R_0 u\rho/\mu$
t	time
t_a	action time
t_b	breakup time
u	gas velocity behind shock wave
u_g	velocity in gas boundary layer
u_l	velocity in liquid boundary layer
$u_{l,av}$	arithmetic average velocity in boundary layer
V	volume of liquid per unit length of jet
V_j	jet velocity
We_0	Weber number based on R_0, $R_0 u^2\rho/\sigma$
x	distance along sheet
y	distance perpendicular to x-axis
α_g	undetermined parameter
α_l	undetermined parameter
δ	boundary-layer thickness
δ_l	liquid boundary-layer thickness
μ	gas viscosity
μ_l	liquid viscosity
ν	kinematic viscosity, μ/ρ
ν_l	liquid kinematic viscosity, μ_l/ρ_l
ρ	gas density behind shock wave

ρ/ρ_1 density ratio across shock

ρ_l liquid density

ρ_1 initial air density

σ interfacial tension

τ_w interface shear stress

ω_n natural frequency of order n

REFERENCES

1. Crocco, Luigi, Harrje, David T., and Reardon, Frederick H.: Transverse Combustion Instability in Liquid Propellant Rocket Motors. ARS Jour. vol. 32, no. 3, Mar. 1962, pp. 366-373.

2. Priem, Richard J., and Guentert, Donald C.: Combustion Instability Limits Determined by a Nonlinear Theory and One-Dimensional Model. NASA TN D-1409, 1962.

3. Webber, W. T.: Spray Combustion in the Presence of a Travelling Wave. Eighth Symposium (International) on Combustion, The Williams & Wilkins Co., 1962, pp. 1129-1140.

4. Cramer, F. B.: The Onset of Detonation in a Droplet Combustion Field. Paper Presented at Ninth Symposium (International) on Combustion, Cornell Univ., Aug. 27-Sept. 1, 1962.

5. Heidmann, Marcus F.: Experimental Effect of Gas Flow Transients on the Heat Release of Burning Liquid Drops in a Rocket Combustor. NASA TN D-1576, 1963.

6. Priem, Richard J., and Morrell, Gerald: Application of Similarity Parameters for Correlating High-Frequency Instability Behavior of Liquid Propellant Combustors. Progress in Astronautics and Rocketry. Vol. 6. - Detonation and Two-Phase Flow. Academic Press, 1962, pp. 305-320.

7. Morrell, Gerald: Critical Conditions for Drop and Jet Shattering. NASA TN D-677, 1961.

8. Crocco, Luigi, and Cheng, Sin-I: Theory of Combustion Instability in Liquid Propellant Rocket Motors. Agardograph 8, Butterworths Sci. Pub. (London), 1956.

9. Morrell, G.: Breakup of Liquid Jets by Transverse Shocks. Eighth Symposium (International) on Combustion, The Williams & Wilkins Co., 1962, pp. 1059-1068.

10. Ames Research Staff: Equations, Tables, and Charts for Compressible Flow. NACA Rep. 1135, 1953. (Supersedes NACA TN 1428.)

11. Engel, Olive G.: Fragmentation of Waterdrops in the Zone Behind an Air Shock. Jour. Res. Nat. Bur. Standards, vol. 60, no. 3, Mar. 1958, pp. 245-280.

12. Taylor, Geoffrey I.: The Shape and Acceleration of a Drop in a High Speed Air Stream. Ptn./6600/5278/49, Chem. Defense Exp. Establishment (Gt. Brit.), 1949.

13. Sandborn, V. A., and Kline, S. J.: Flow Models in Boundary-Layer Stall Inception. Trans. ASME, Jour. Basic Eng., ser. D, vol. 83, no. 3, Sept. 1961, pp. 317-327.

TABLE I. - BREAKUP DATA FOR SINGLE WATER JETS

Run	Jet diameter, in.	Shock velocity, ft/sec	Breakup time, msec	Jet velocity, ft/sec	Action time, msec	Gas velocity behind shock, ft/sec	Shocked gas density, lb/cu ft	Natural period of jet, $2\pi/\omega_2$, msec
Length of high-pressure section, 1 in.								
[a]81	0.018	1670	0.52	46	1.05	750	0.137	1.04
82	.018	1425	.63	46	.79	440	.109	1.04
83	.018	1260	1.29	46	[b].6	210	.0875	1.04
85	.052	1170	(c)	39.4	.53	62	.0795	5.1
86	↓	1270	(c)	39.4	.63	225	.0898	↓
87	↓	1440	.9	39.4	.84	458	.11	↓
88	↓	1657	.72	39.4	1.05	732	.134	↓
89	.0785	1145	(c)	33	.74	25	.077	9.45
90	↓	1240	(c)	33	.46	175	.087	↓
91	↓	1430	1.54	33	.42	445	.109	↓
92	↓	1680	.96	33	.84	762	.137	↓
Length of high-pressure section, 6 in.								
153	0.052	1220	5.4	39.4	2.25	147	0.0845	5.1
154	↓	1365	1.8	39.4	1.5	357	.101	↓
155	↓	1635	1.3	39.4	2.5	707	.132	↓
156	↓	1880	.7	39.4	2.5	1000	.159	↓
157	.018	1870	.53	46	2.25	992	.159	1.04
158	↓	1660	.8	46	1.9	737	.135	↓
159	↓	1355	.94	46	1.25	345	.10	↓
160	↓	1236	1.53	46	1.0	173	.086	↓
161	.0785	1256	(c)	33	[b].9	200	.0885	9.45
163	.0785	1670	1.57	33	1.3	750	.137	9.45
164	.0785	1890	.97	33	2.25	1010	.161	9.45
165	.157	1875	1.56	19.7	2.7	995	.159	26.8
167	.157	1375	(c)	19.7	1.7	373	.103	26.8
[d]195	.018	1354	.3	46	.7	345	.10	1.04
196	.018	1675	.15	46	1.1	755	.137	1.04
197	.018	1875	.12	46	2.0	995	.159	1.04
198	.052	1888	.4	39.4	2.2	1010	.161	5.1
199	↓	1654	.5	39.4	1.2	730	.135	↓
200	↓	1350	.91	39.4	1.0	340	.0995	↓
201	↓	1231	3.01	39.4	[b].9	165	.086	↓
202	.0785	1235	(c)	33	[b]1.0	172	.086	9.45
203	.0785	1348	1.42	33	.43	335	.099	9.45
204	.0785	1679	1.08	33	1.44	760	.137	9.45
206	.157	1855	1.59	19.7	2.31	972	.157	26.8
207	.157	1662	2.1	19.7	1.25	740	.1355	↓
208	.157	1358	(c)	19.7	[b]1.0	347	.10	↓

[a]Runs 81-92 and 153-167: framing photographs taken with 100-mm lens.

[b]Estimated.

[c]Incomplete breakup.

[d]Runs 195-208: streak photographs.

TABLE I. - Concluded. BREAKUP DATA FOR SINGLE WATER JETS

Run	Jet diameter, in.	Shock velocity, ft/sec	Breakup time, msec	Jet velocity, ft/sec	Action time, msec	Gas velocity behind shock, ft/sec	Shocked gas density, lb/cu ft	Natural period of jet, $2\pi/\omega_2$, msec
Length of high-pressure section, 2 ft								
[a]59	0.018	1255	0.61	46	[b]3.75	200	0.0884	1.04
60		1376	.53	46	[b]4	370	.102	
61		1690	.36	46	5.6	775	.139	
62		2000	.13	46	6.8	1135	.172	
63	.052	1937	.42	39.4	[b]6	1065	.166	5.1
64		1677	.54	39.4	4.7	757	.137	
65		1380	1.05	39.4	4.1	380	.102	
66		1270	1.88	39.4	3.6	225	.0898	
67	.0785	1260	2.49	33	4.2	210	.0884	9.45
68	.0785	1370	1.49	33	4.4	365	.102	9.45
73	.157	1395	2.3	19.7	4.7	400	.104	26.8
74		1267	5.2	19.7	3.9	220	.0898	
[c]147		1635	2	19.7	4.75	707	.133	
148		1880	1.4	19.7	4.9	1000	.16	
149	.0785	1865	1	33	5.5	987	.158	9.45
150	.0785	1630	1.4	33	4.7	700	.132	9.45
151	.052	1655	1	39.4	4.4	733	.134	5.1
152	.052	1880	.6	39.4	5.5	1000	.16	5.1
Length of high-pressure section, 8 ft								
[d]97	0.157	1250	5.2	19.7	[b]15.1	195	0.087	26.8
98	.157	1370	2.9	19.7	[b]15.8	365	.103	26.8
104	.0785	1370	1.69	33	[b]15.8	365	.103	9.45
105	.0785	1253	2.2	33	[b]15.1	198	.088	9.45
106	.052	1267	2.5	39.4	[b]15.3	220	.0898	5.1
107		1370	1.4	39.4	[b]15.8	365	.102	
108		1660	.5	39.4	12.7	737	.135	
109		1875	.5	39.4	16.2	1000	.16	
110	.018	1875	.3	46	16.5	1000	.16	1.04
111		1650	.3	46	13.1	725	.134	
112		1377	.7	46	[b]15.8	375	.1025	
113		1290	1.15	46	16.3	255	.092	
[e]136		1870	.5	46	19.5	992	.16	
137		1653	.7	46	18.0	727	.134	
138	.052	1365	1.9	39.4	14.6	357	.102	5.1
139	.052	1660	1.1	39.4	18.0	737	.135	5.1
140	.052	1855	.9	39.4	19.4	970	.157	5.1
141	.0785	1870	1.1	33	18.25	992	.159	9.45
142	.0785	1645	1.43	33	18.5	720	.134	9.45
143	.157	1245	7.0	19.7	12.3	187	.0875	26.8
144		1355	4.1	19.7	18.4	345	.1	
145		1642	1.8	19.7	18.3	715	.133	
146		1865	1.3	19.7	17.2	987	.158	
[f]210		1240	5.9	19.7	[b]15.1	180	.088	
211		1350	3.3	19.7	[b]15.7	337	.10	
212		1630	1.9	19.7	[b]17	700	.132	
213		1820	1.4	19.7	24.9	935	.153	
214	.0785	1830	1.0	33	19.5	945	.155	9.45
215		1635	1.45	33	19.6	707	.133	
216		1360	2.21	33	15.9	350	.101	
217		1256	3.05	33	16.8	200	.0885	
218	.052	1240	1.91	39.4	17.4	180	.088	5.1
219		1325	1.21	39.4	16.3	305	.097	
220		1652	1.03	39.4	18.3	727	.134	
221		1870	.75	39.4	18.9	992	.159	
222	.018	1835	.28	46	18.9	950	.155	1.04
223		1647	.19	46	16.3	720	.134	
224		1360	.4	46	13.7	350	.101	
225		1240	.9	46	13.6	180	.088	

[a]Runs 59-74: framing photographs taken with 100-mm lens.

[b]Estimated.

[c]Runs 147-152: framing photographs taken with 50-mm lens.

[d]Runs 97-113: framing photographs taken with 100-mm lens.

[e]Runs 136-146: framing photographs taken with 50-mm lens.

[f]Runs 210-225: streak photographs.

TABLE II. - BREAKUP DATA FOR 0.052-INCH-DIAMETER JET FORMED AT SHARP-EDGED ORIFICE

Run	Shock velocity, ft/sec	Breakup time, msec	Action time, msec	Gas velocity behind shock, ft/sec	Shocked gas density, lb/cu ft
Length of high-pressure section, 1 in.					
[a]78	1257	(b)	0.63	202	0.0875
79	1425	0.7	.84	440	.109
80	1670	.6	1.05	750	.137
Length of high-pressure section, 2 ft					
75	1390	1.07	4.4	392	0.103
76	1668	.6	5.3	748	.135
Length of high-pressure section, 8 ft					
114	1253	2.06	13.4	198	0.09
115	1367	1.19	12.9	360	.101
116	1657	.6	13.4	732	.134
117	1890	.3	17.2	1015	.161
[c]133	1670	1.06	16.6	750	.137
134	1663	1.08	16.6	742	.136
135	1855	.9	18.6	970	.157

[a]Runs 78-80, 75-76, 114-117: framing photographs taken with 100-mm lens.

[b]Breakup incomplete.

[c]Runs 133-135: framing photographs taken with 50-mm lens.

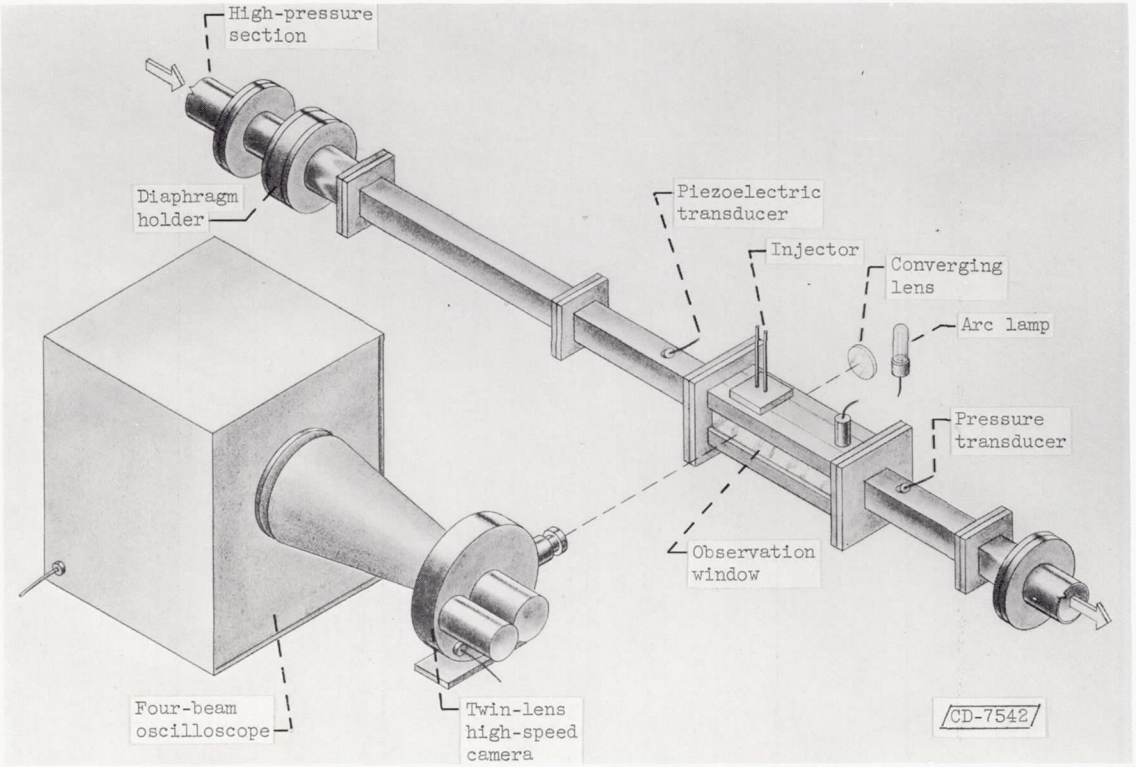

(a) Schematic diagram of experimental arrangement.

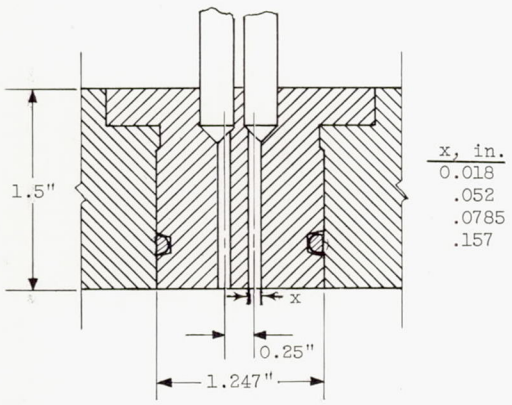

x, in.
0.018
.052
.0785
.157

(b) Large L/D injector configuration.

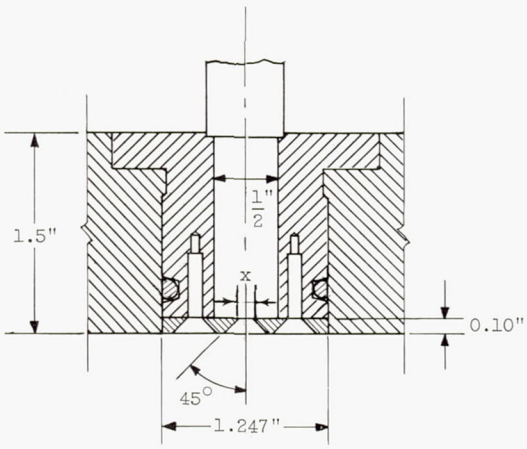

(c) Sharp-edged orifice injector.

Figure 1. - Experimental arrangement and injector configurations.

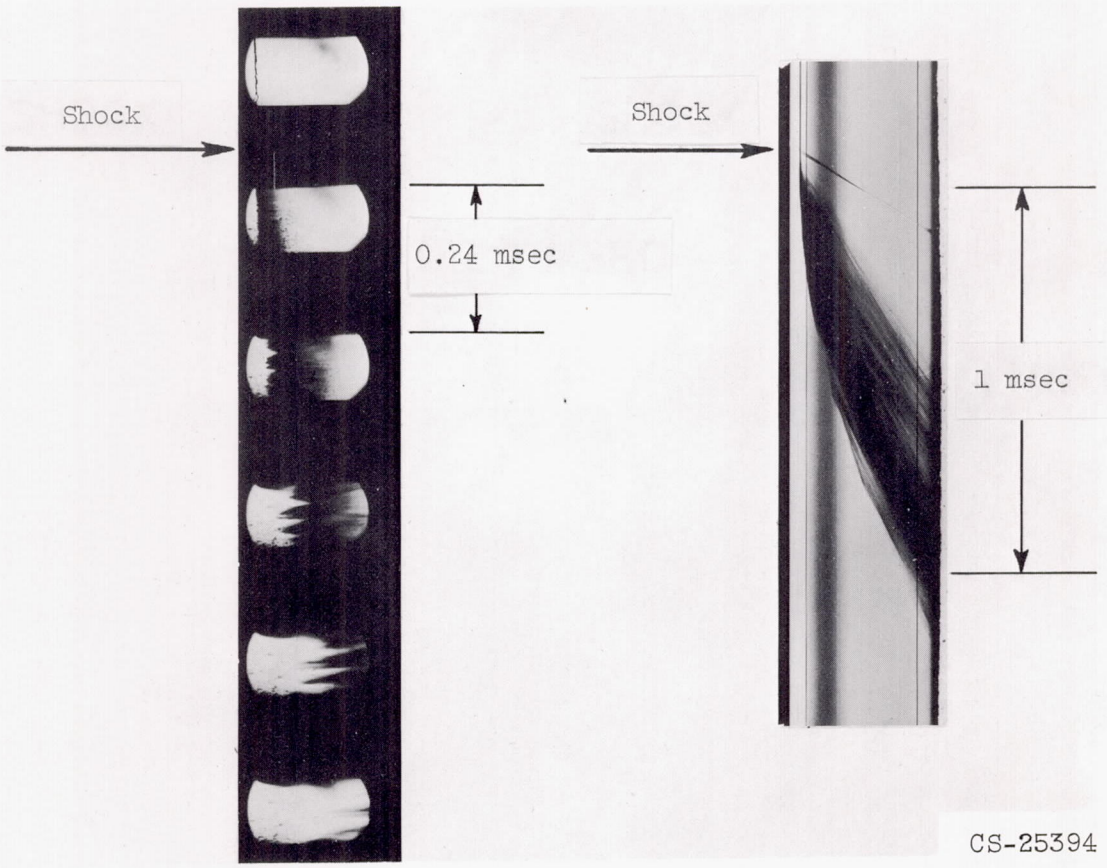

Figure 2. - Examples of photographic data of jet breakup. Shock velocity, 1655±5 feet per second; gas velocity, 732±5 feet per second; jet diameter, 0.052 inch; breakup time, ~1.1 milliseconds.

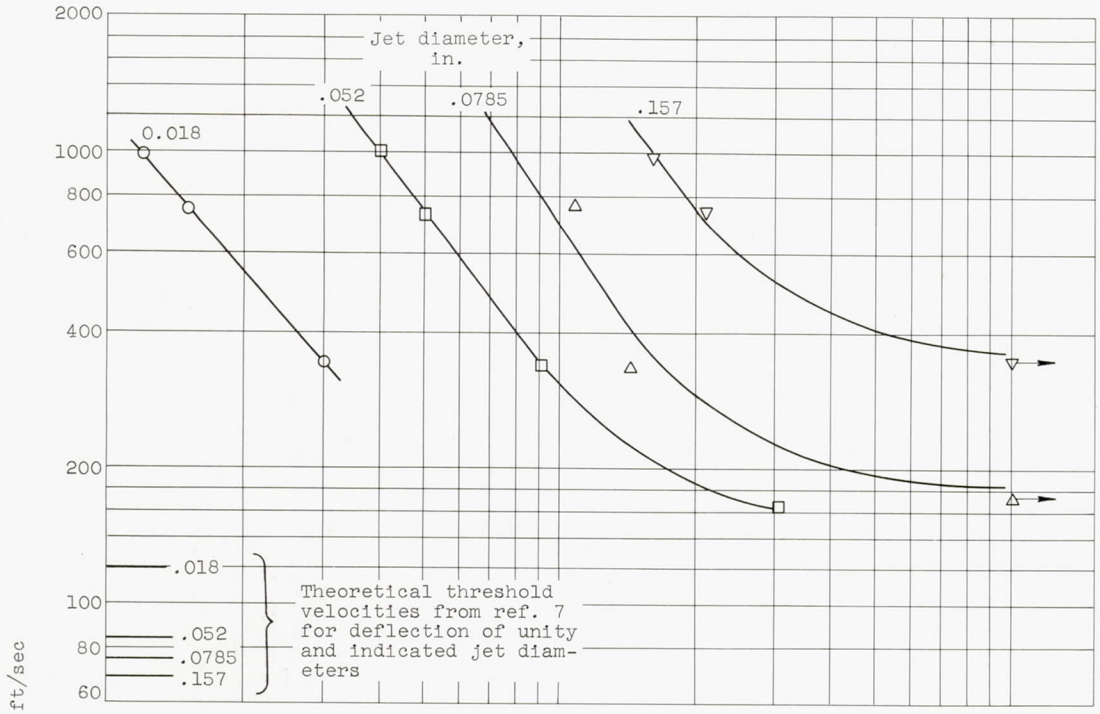

(a) High-pressure-section length, 6 inches; action time, 1-2 milliseconds.

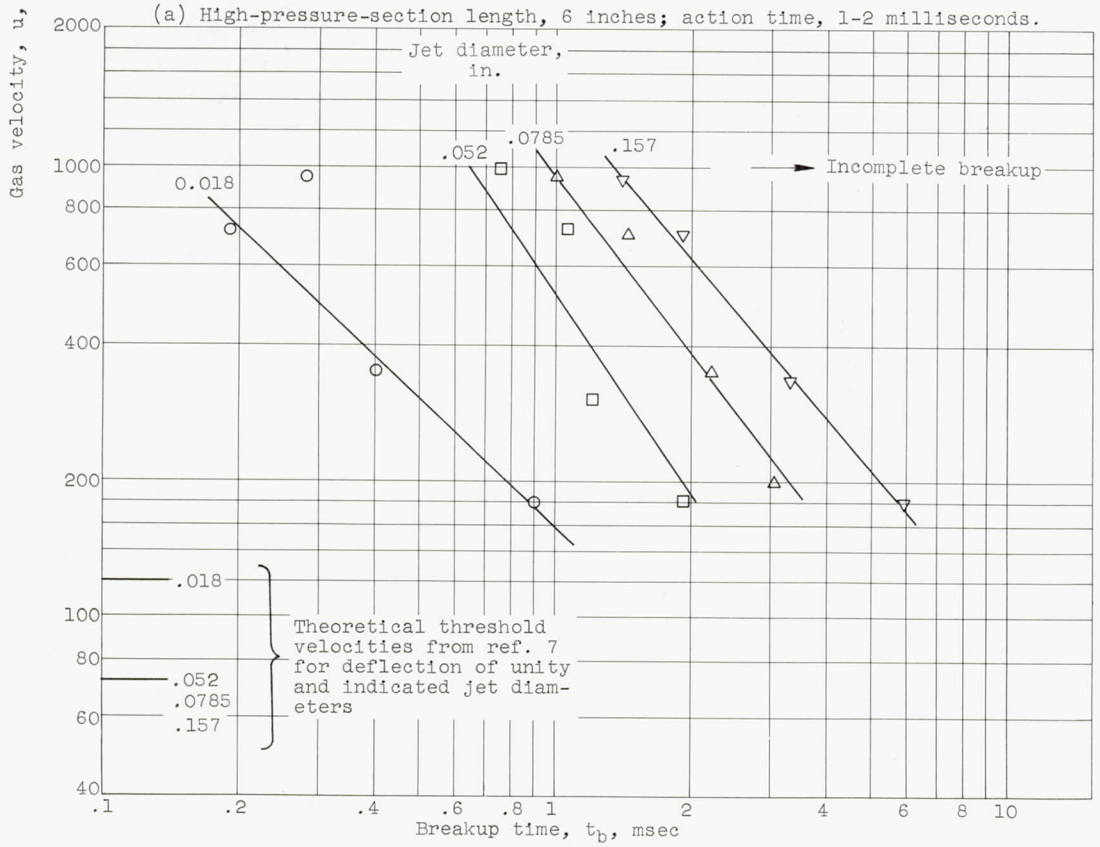

(b) High-pressure-section length, 8 feet; action time, 13-20 milliseconds.

Figure 3. - Dependence of breakup time on gas velocity.

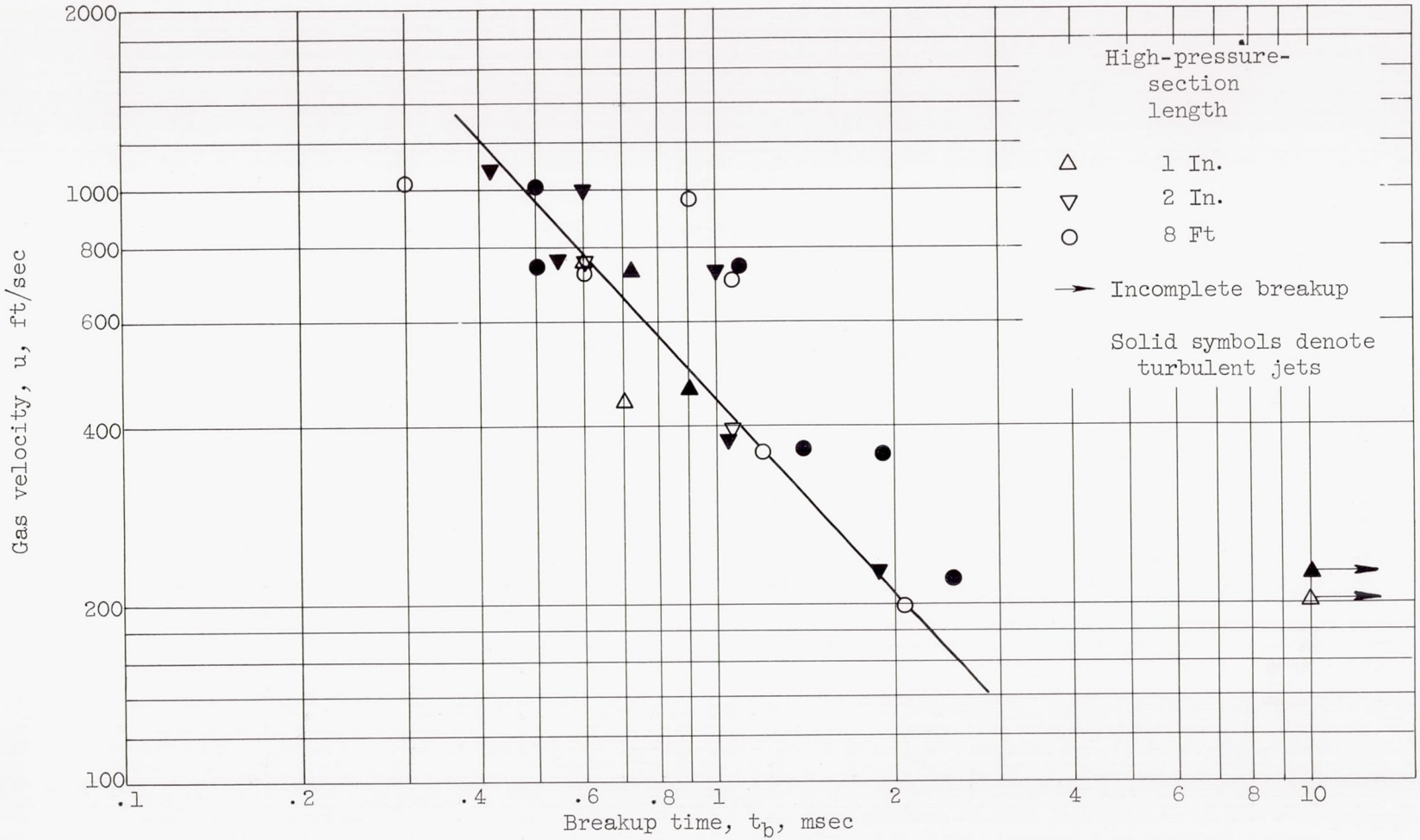

Figure 4. - Breakup times for 0.052-inch-diameter jet formed by sharp-edged orifice.

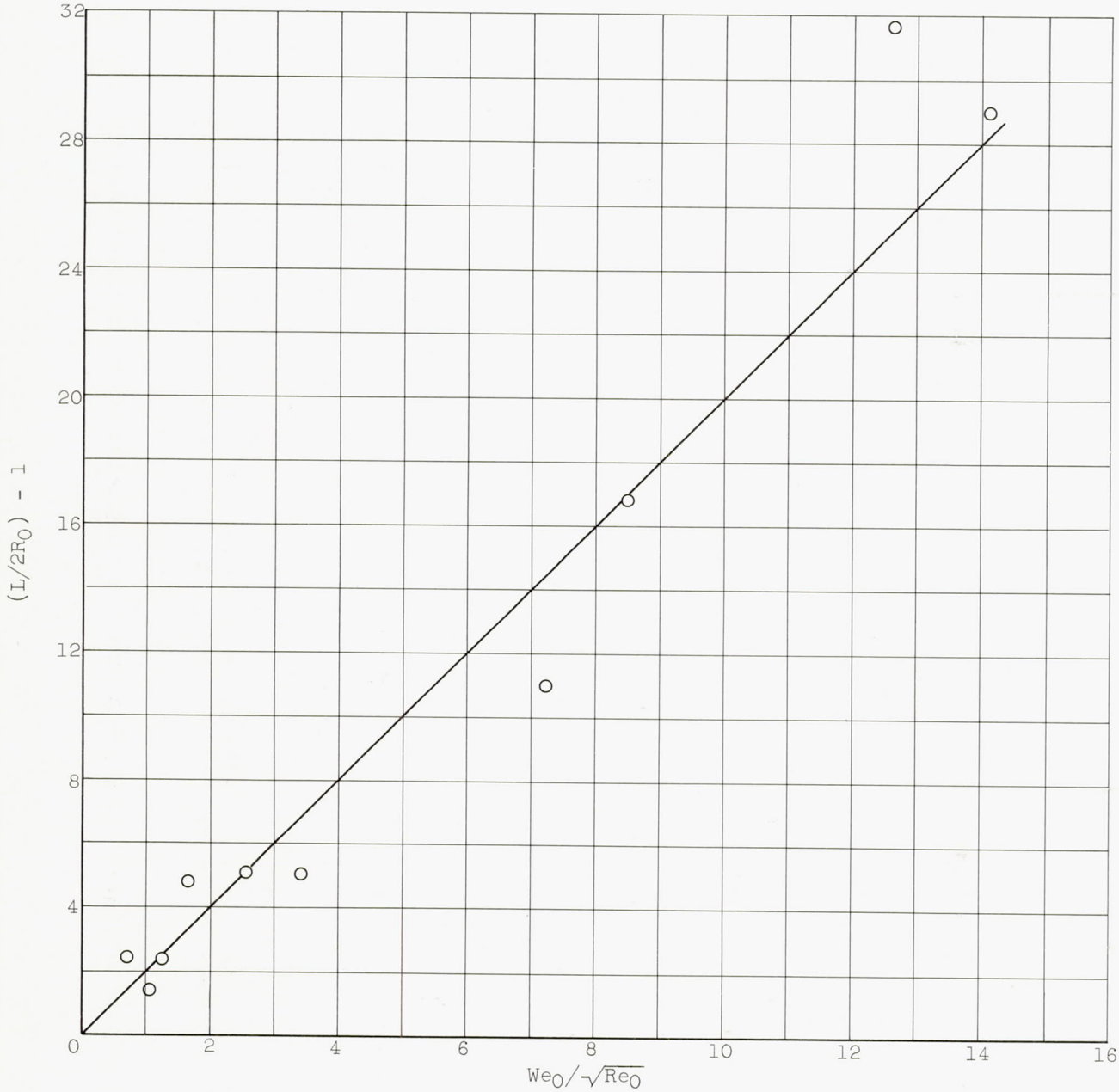

Figure 5. - Maximum apparent sheet length of liquid mass plotted as a function of Weber number and Reynolds number.

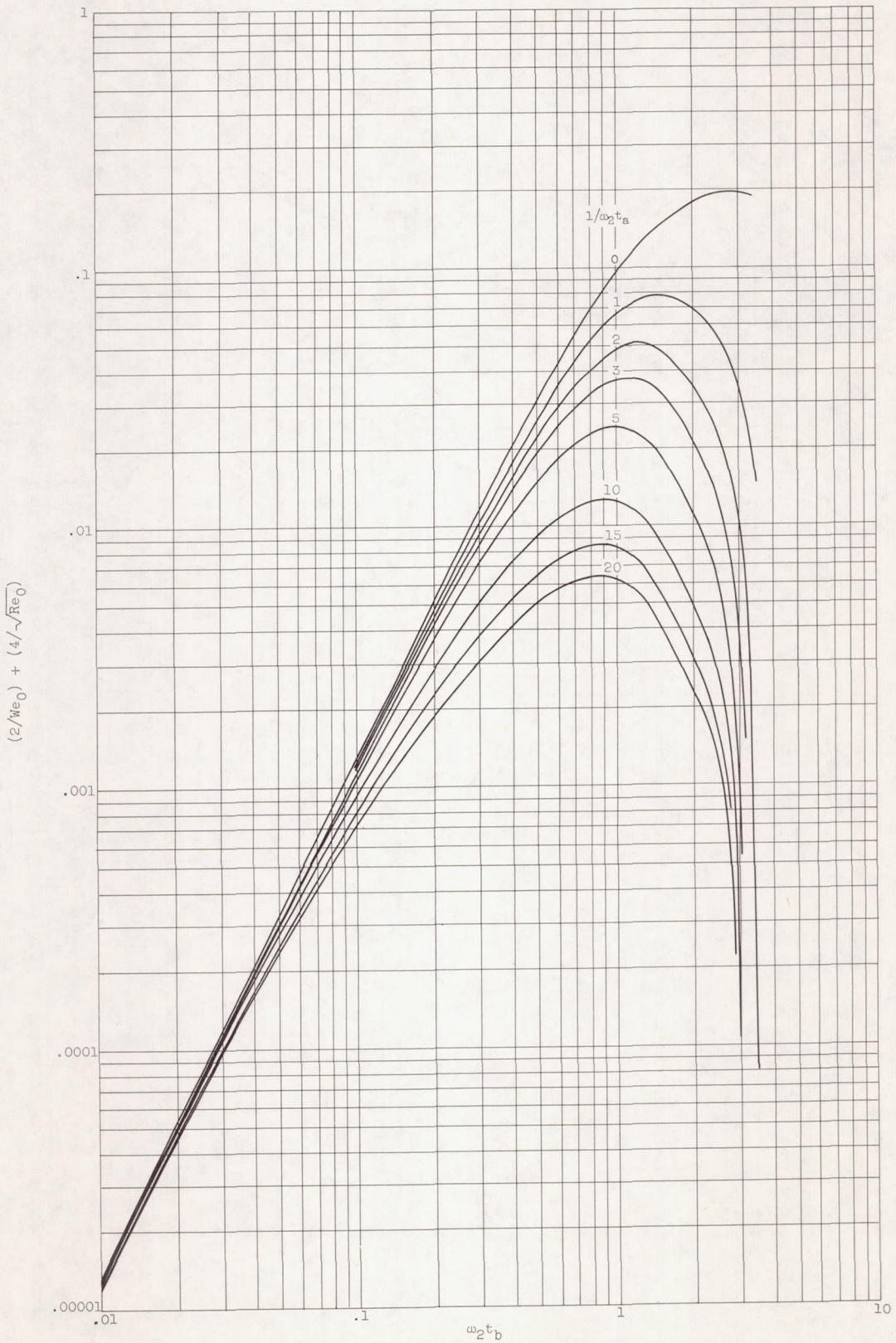

Figure 6. - Plot of expression for breakup time according to deformation model.

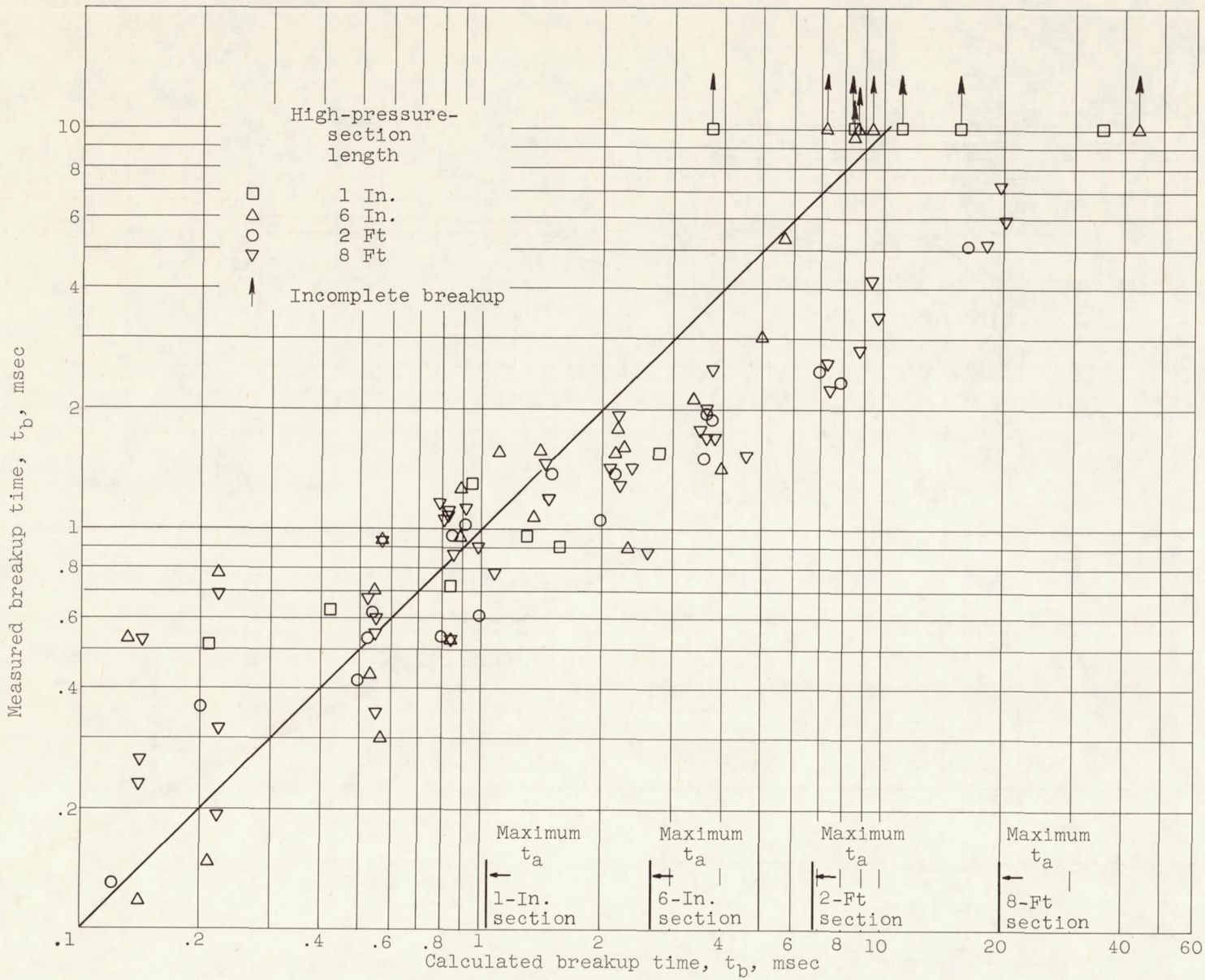

(a) According to boundary-layer model.

Figure 7. - Comparison of measured and calculated values of breakup time.

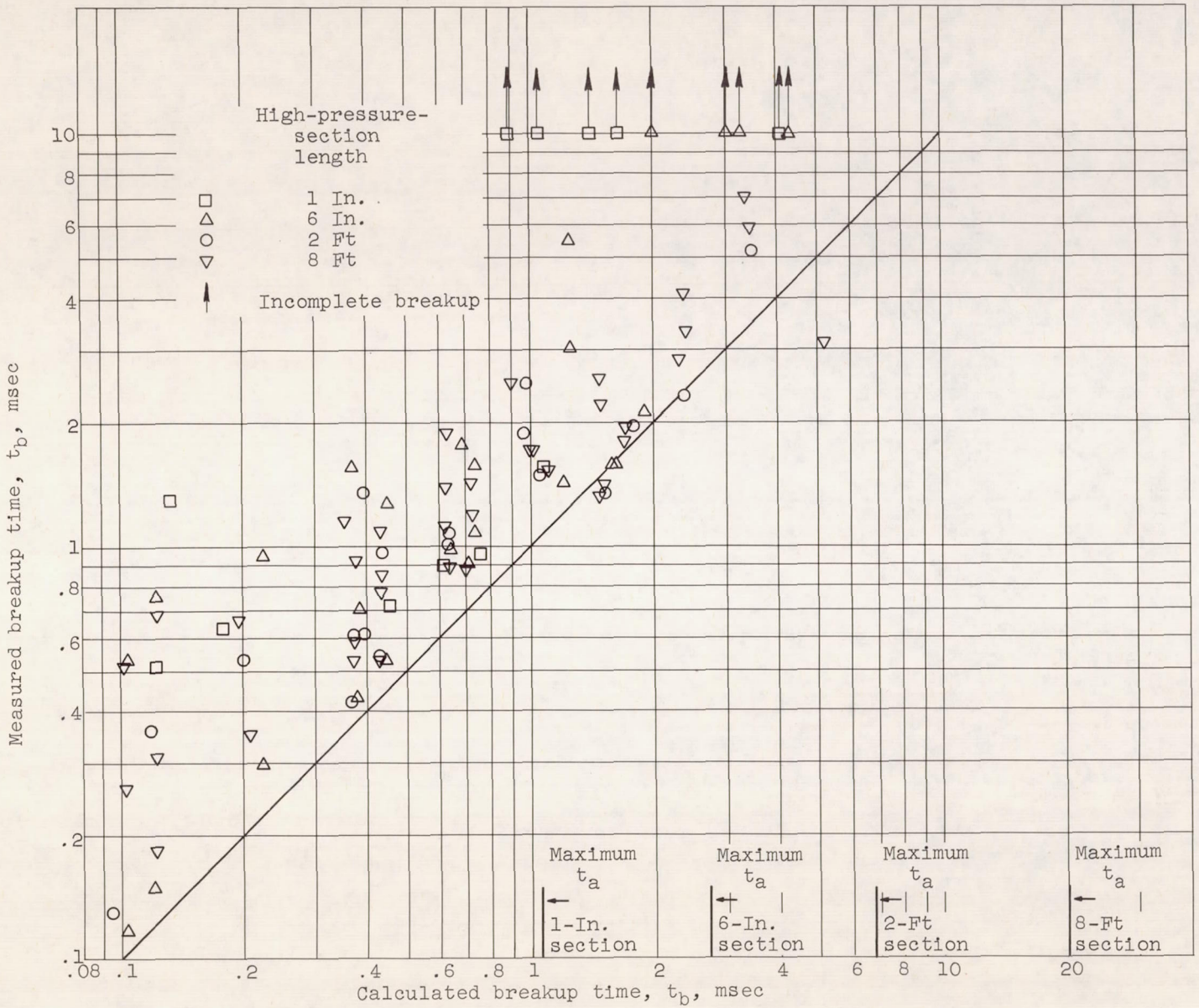

(b) According to deformation model.

Figure 7. - Concluded. Comparison of measured and calculated values of breakup time.